

Modern Interferometry

Kym Derriman, James Ammerlaan, and Kevin Gonzalez
Rutgers University
(Dated: January 7, 2026)

This experiment used the TeachSpin Modern Interferometry system to investigate several applications of optical interferometry. A Michelson interferometer was aligned and used to measure the wavelength of a HeNe laser, the pressure dependence of the refractive index of air, and the refractive index of a quartz slab. A Sagnac interferometer was also partially assembled, although the full procedure could not be completed due to equipment malfunction.

I. INTRODUCTION

Optical interferometry measures phase differences between coherent beams that traverse different optical paths. Because a 2π phase shift corresponds to a path difference of one wavelength, interferometers are sensitive to small changes in distance and refractive index. In this experiment, a Michelson interferometer was used to determine the wavelength of a HeNe laser and to measure refractive index changes produced by varying the air pressure in one arm. The same fringe-counting method was used to determine the refractive index of quartz. A Sagnac interferometer was also assembled to examine rotation-sensitive interferometry, though full measurements were not possible due to equipment issues.

II. THEORY

Michelson Interferometer and Refractive Index Changes

In a Michelson interferometer, the beamsplitter divides the incident beam into two perpendicular arms of lengths L_1 and L_2 . After reflection and recombination, the phase difference between the two beams is

$$\Delta\phi = \frac{2\pi}{\lambda} 2(L_1 - L_2), \quad (1)$$

where the factor of 2 accounts for the round trip in each arm.

A change in optical path difference of λ produces one full fringe shift (e.g., from one bright maximum to the next). Thus, if the mirror in one arm is displaced by dx , the change in optical path difference is

$$\Delta(\text{OPL}) = 2 dx = m\lambda, \quad (2)$$

where m is the number of fringes counted. If the mirror moves at speed $v = dx/dt$ and the measured fringe rate is $n = dm/dt$, then

$$\lambda = \frac{2v}{n}. \quad (3)$$

When a medium of refractive index n and physical length L is inserted into one arm, the optical path length

through that arm becomes

$$\text{OPL} = nL. \quad (4)$$

A change in refractive index Δn produces a change in optical path length

$$\Delta(\text{OPL}) = 2L \Delta n, \quad (5)$$

again including the factor of 2 for the double pass. Since each fringe corresponds to a change $\Delta(\text{OPL}) = \lambda$, a measured fringe shift m satisfies

$$\Delta(\text{OPL}) = m\lambda. \quad (6)$$

Equating these expressions gives the index-change relation

$$\Delta n = \frac{m\lambda}{2L}. \quad (7)$$

Refractive Index of Transparent Slabs

To measure the refractive index of a transparent slab, a slab of thickness t is inserted into one arm of the interferometer at near-normal incidence. The slab is then rotated by a small angle θ (in radians), which introduces a change in the optical path length due to the increased geometrical path through the material. For small θ , this change can be approximated as

$$\Delta(\text{OPL}) \approx (n - 1) t \theta^2, \quad (8)$$

where the approximation arises from the small-angle expansion of the beam's traversal path, accounting for refraction and the double pass in the Michelson configuration.

Since each observed fringe shift m corresponds to a change in optical path length of $m\lambda$, we have

$$\Delta(\text{OPL}) = m\lambda. \quad (9)$$

Equating the two expressions yields

$$(n - 1) t \theta^2 = m\lambda, \quad (10)$$

which rearranges to give the refractive index

$$n = 1 + \frac{m\lambda}{t \theta^2}. \quad (11)$$

III. EXPERIMENTAL SETUP

All measurements were performed using the TeachSpin Modern Interferometry system operated in a Michelson configuration. A He–Ne laser provided the coherent source. Two steering mirrors directed the beam to a 50/50 beamsplitter, which formed the two interferometer arms. Each arm terminated in a mirror, and the recombined beam was directed to a photodiode detector. A narrow slit was applied to the photodiode face using black tape to prevent saturation and permit clean fringe detection.

For wavelength measurements, one of the end mirrors was mounted on a motorized translation stage capable of uniform motion at a fixed velocity.

For measurements involving a controlled change in optical path length, two components were inserted into the arm between the beamsplitter and Mirror 2: (i) a 1.5-inch gas cell equipped with a hand pump and pressure gauge, and (ii) a quartz slab mounted on a rotation stage for refractive-index measurements. (The glass sample provided with the apparatus could not be made to produce stable, countable fringes and was therefore not used in the analysis.)

A separate three-mirror loop was also assembled in an attempt to configure a Sagnac interferometer using the provided non-polarizing beamsplitter cube.

IV. PROCEDURE

A. Wavelength Measurement

The Michelson interferometer was aligned to produce stable fringes at the photodiode detector. The viewing screen was removed and replaced with the slit-modified photodiode, which was connected to an oscilloscope. Figure 1 shows the translation-stage assembly used for the wavelength measurement.

The mirror mounted on the translation stage was driven over a measured distance to determine the stage velocity. With the velocity calibrated, the stage was driven at constant speed while the photodiode signal was recorded. The periodic intensity modulation in the oscilloscope trace was later used to determine the fringe frequency.

B. Refractive Index of Air

A 1.5-inch gas cell was inserted into one arm of the interferometer. After alignment, the cell was pressurized using the hand pump. The exhaust valve was then opened slightly to allow a slow and steady decrease in pressure, producing a uniform drift of interference fringes. The photodiode output and the initial and final cell pressures were recorded.



FIG. 1. Michelson interferometer arm containing the motorized translation stage and fine-adjustment mount used for wavelength measurements. The mirror on this stage was translated at a calibrated constant velocity to generate measurable fringe motion.

C. Refractive Index of Transparent Slabs

A quartz slab of thickness 1 mm was mounted on the rotation stage and inserted into the interferometer arm between the beamsplitter and Mirror 2. After alignment, the slab was rotated by a small angle to introduce a controlled change in optical path length, producing a measurable fringe shift. The rotation angle and corresponding fringe count were recorded for later determination of the refractive index. (The glass sample supplied with the apparatus did not yield stable, countable fringes and was therefore not used.)

D. Sagnac Interferometer Attempt

A triangular Sagnac configuration was assembled using three mirrors and a non-polarizing beamsplitter cube. The intended beam paths and layout are shown in Fig. 2. Alignment was attempted to produce counter-propagating beams around the loop; however, mechanical instability in two mounts and insufficient overlap of the returning beams prevented the formation of observable Sagnac fringes. No quantitative measurements were obtained.

V. RESULTS

A. Wavelength Measurement

Stable interference fringes were recorded at the photodiode with the translation stage driven at constant velocity. The mirror velocity was determined from three tim-

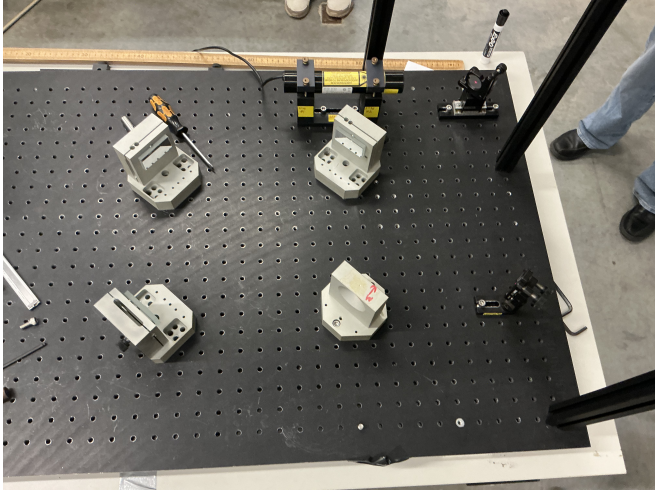


FIG. 2. Attempted Sagnac interferometer assembly. Counter-propagating beams could not be stably overlapped due to mechanical instability, preventing observation of Sagnac fringes.

ing measurements of the stage motion, yielding a mean value of

$$v = (8.52 \pm 0.23) \times 10^{-7} \text{ m/s.}$$

Three oscilloscope waveforms were recorded during the wavelength runs. Each file contained a region of uniform fringe motion suitable for counting. A representative trace is shown in Fig. 3.

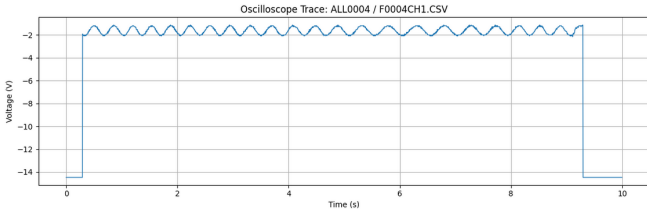


FIG. 3. Photodiode voltage versus time during a wavelength run. The periodic modulation corresponds to fringes produced as the translation-stage mirror moved at constant velocity.

From the three selected runs, the number of fringes passing the photodiode during a known time interval was measured. The resulting fringe frequencies were

$$n_1 = 2.75 \text{ Hz}, \quad n_2 = 2.333 \text{ Hz}, \quad n_3 = 2.50 \text{ Hz.}$$

These values were used to obtain a mean fringe rate for the wavelength calculation.

B. Refractive Index of Air

With the gas cell inserted, stable fringes were again obtained. As the air was slowly vented from the cell, the

photodiode recorded a steady fringe motion. Figure 4 shows a representative portion of the recorded waveform during a pressure decrease.

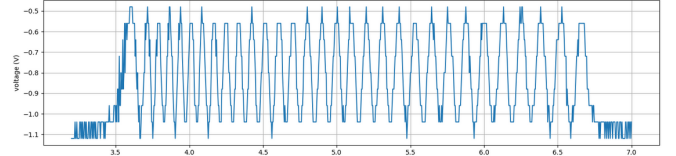


FIG. 4. Fringe motion recorded during slow pressure release from the gas cell. The number of fringes passing the detector was counted from this waveform and compared with the measured pressure change.

For the first run, a total of 31 fringes passed during a recorded pressure change of 13 psi. These measurements were used to compute the change in optical path length and the corresponding change in refractive index (Sec. VI).

C. Refractive Index of Transparent Slabs

A quartz slab of thickness $t = 1 \text{ mm}$ was inserted into one arm of the interferometer and rotated by a small angle. A rotation of 4° produced a measurable fringe shift of approximately $m = 4.5$ fringes. These quantities were used to determine the refractive index of the quartz slab as described in Sec. VI.

VI. ANALYSIS

A. Wavelength Measurement

The wavelength was determined using the standard Michelson relation,

$$\lambda = \frac{2v}{n} \quad (12)$$

where v is the calibrated mirror velocity and n is the fringe frequency extracted from the oscilloscope traces.

The three timing measurements of the translation stage gave

$$v = (8.52 \pm 0.23) \times 10^{-7} \text{ m/s.}$$

Using the fringe counts from the three oscilloscope files,

$$n_1 = 2.75 \text{ Hz}, \quad n_2 = 2.333 \text{ Hz}, \quad n_3 = 2.50 \text{ Hz,}$$

the mean and standard deviation were

$$n = 2.528 \pm 0.21 \text{ Hz.}$$

Substituting these into Eq. (12) gives

$$\lambda = \frac{2(8.52 \times 10^{-7})}{2.528} = 6.74 \times 10^{-7} \text{ m} = 674 \text{ nm.}$$

Uncertainty propagation yields

$$\sigma_\lambda = 5.9 \times 10^{-8} \text{ m} = 59 \text{ nm.}$$

Thus the final result is

$$\lambda = (674 \pm 59) \text{ nm,}$$

which is consistent with the nominal He–Ne wavelength of 633 nm.

B. Refractive Index of Air

Using the relation derived in the Theory section,

$$\Delta n = \frac{m\lambda}{2L}, \quad (13)$$

and the measured values for the first run

$$m = 31, \quad \Delta P = 13 \text{ psi,}$$

together with the nominal He–Ne wavelength

$$\lambda = 633 \text{ nm} = 6.33 \times 10^{-7} \text{ m,}$$

and the gas cell length

$$L = 1.5 \text{ in} = 0.0381 \text{ m,}$$

we compute

$$m\lambda = 31 \times 6.33 \times 10^{-7} = 1.96 \times 10^{-5} \text{ m,}$$

$$\Delta n = \frac{1.96 \times 10^{-5}}{2 \times 0.0381} = 2.58 \times 10^{-4}.$$

The change in refractive index per unit pressure is

$$\frac{\Delta n}{\Delta P} = \frac{2.58 \times 10^{-4}}{13} = 2.0 \times 10^{-5} \text{ psi}^{-1}.$$

The corresponding change in optical path per unit pressure is

$$\frac{\Delta(\text{OPL})}{\Delta P} = \frac{1.96 \times 10^{-5}}{13} = 1.51 \times 10^{-6} \text{ m/psi.}$$

C. Refractive Index of Transparent Slabs

Using the small-angle slab-rotation relation

$$n = 1 + \frac{m\lambda}{t\theta^2}, \quad (14)$$

the refractive index of the quartz slab was determined from the measured values $t = 1 \text{ mm} = 0.001 \text{ m}$, $\theta = 4^\circ = 0.0698 \text{ rad}$, $m \approx 4.5$, and $\lambda = 633 \text{ nm}$. With $\theta^2 \approx 4.87 \times 10^{-3}$, $t\theta^2 \approx 4.87 \times 10^{-6} \text{ m}$, and $m\lambda \approx 2.85 \times 10^{-6} \text{ m}$, the resulting index is

$$n_{\text{quartz}} \approx 1.58.$$

No usable data were obtained for the glass sample, as stable, countable fringes could not be produced.

VII. DISCUSSION

The measurements performed with the Michelson interferometer demonstrate both the strengths and practical limitations of fringe based optical metrology. Each component of the experiment produced results that were qualitatively consistent with theory. However, the Michelson interferometer struggled to remain accurate, as any very minute changes could result in large scale errors seen in fringe counts.

The wavelength measurement produced a value of $\lambda = (674 \pm 59) \text{ nm}$, which overlaps with the known value of the HeNe laser wavelength of 633 nm. The central value found is higher than expected, but this is a consequence of our uncertainty of the translation stage motor velocity due to some slippage occurring. This produced times of slowing down and then speeding up within the fringe count. Even with this instrument issue, our wavelength being within one uncertainty is fairly accurate.

The refractive index measurement for air also followed the expected trend: decreasing the pressure within the gas cell produced a steady change of fringes as the pressure decreased in the system. This is expected as the index of refraction of the air changes with pressure, causing a change in the effective optical path length of the arm. The extracted change in refractive index per unit of pressure was about $\frac{\Delta n}{\Delta P} = 2 \times 10^{-5} \text{ psi}^{-1}$. This calculation is within the correct order of magnitude for air in near atmospheric conditions. The dominant source of uncertainty in the experiment is the assumption that the pressure system to pressurize and depressurize the system was purely linear. Meaning that when the chamber started to depressurize it didn't do so at the same rate constantly but instead slowed as the chamber depressurized. To improve upon this experiment, we recommend using a digital pressure sensor to gather more accurate readings and a pressure system that can release at a given constant rate.

The slab rotation experiment produced fragile fringes, which demonstrate the relation shown in Eq. (11). However, the system relied heavily on the rotation stage that was incredibly hard to create a method that didn't interfere with the whole system. These effects such as the slightest graze of the baseboard or rotating too quickly or slowly created skewed results. This essentially made it impossible to count the fringes of the glass sample but were able to gently gather enough data with the quartz sample. This data allowed us to find a value close to the expected range for a quartz sample, but slightly higher than typical values, potentially due to experimental approximations.

Finally, the attempted Sagnac interferometer highlights the differences between it and the Michelson version. Whilst entirely more stable due to its configuration, the precision of all parts needed to complete the system is higher. This was the issue when setting up and calibrating the system. Small movements created a shift through both arms and polarization also created

further issue. This does not contradict what we know about Sagnac interferometers but instead reinforces their biggest strength and weakness of rotational sensitive interferometry.

VIII. CONCLUSION

The Modern Interferometry experiments successfully showed how phase-sensitive optical measurements can be used to measure other physical quantities with high qual-

ity. Using the Michelson interferometer, we measured the wavelength of the HeNe laser, the pressure-refractive index relation of air, and how it can be used to find the refractive index of solid slabs. Although mechanical limitations and sensitivities of equipment introduced large uncertainties, all results were consistent with predictions within experimental tolerance. The attempt to assemble a Sagnac interferometer only demonstrated the level of calibration needed to configure it and its stability when assembled. Overall, the experiments highlighted the power of using light to measure other quantities with high precision.

-
- [1] Rutgers University, Department of Physics and Astronomy, *Modern Interferometry Laboratory Manual* (2025).
 - [2] E. Hecht, *Optics*, 5th ed. (Pearson, Boston, 2017).
 - [3] F. L. Pedrotti, L. M. Pedrotti, and L. S. Pedrotti, *Introduction to Optics*, 3rd ed. (Pearson Prentice Hall, Upper Saddle River, 2007).
 - [4] R. P. Feynman, R. B. Leighton, and M. Sands, *The Feynman Lectures on Physics*, Vol. I–III (Addison–Wesley, Reading, MA, 1964).
 - [5] J. A. Stone and J. H. Zimmerman, “Refractive Index of Air Calculator,” National Institute of Standards and Technology (NIST). Available at <https://emtoolbox.nist.gov/wavelength/documentation.asp>.